

10

15

20

25

30

Title: Fluid-induced aseismic fault slip outpaces pore-fluid migration

Authors: Pathikrit Bhattacharya^{1,2*}, Robert C. Viesca^{1*}.

Affiliations:

¹Department of Civil and Environmental Engineering, Tufts University, Medford, Massachusetts 02155, USA.

²School of Earth, Ocean and Climate Sciences, Indian Institute of Technology Bhubaneswar, Argul, Odisha 752050, India

*Correspondence to: path_geoalum@alumni.princeton.edu, robert.viesca@tufts.edu.

Abstract: Earthquake swarms attributed to subsurface fluid-injection are usually assumed to occur on faults destabilized by elevated pore-fluid pressures. However, fluid injection could also activate aseismic slip, which might outpace pore-fluid migration and transmit earthquake-triggering stress changes beyond the fluid-pressurized region. We test this theoretical prediction against data derived from fluid-injection experiments that activated and measured slow, aseismic slip on pre-existing, shallow faults. We found that the pore-pressure and slip history imply a fault whose strength is the product of a slip-weakening friction coefficient and the local effective normal stress. Using a coupled shear-rupture model, we derive constraints on the hydro-mechanical parameters of the actively deforming fault. The inferred aseismic rupture front propagates faster and to larger distances than the diffusion of pressurized pore fluid.

One Sentence Summary: Fluid-fault interaction inferred from in situ data.

Main Text:

Fluid injections related to geothermal or oil and gas operations are associated with enhanced local seismicity rates (1–8). These earthquakes often occur as an enlarging cloud of seismicity migrating away from the point of injection (9, 10). The cloud's diffusive growth is usually interpreted as representing the diffusion of elevated pore fluid pressure reaching pre-stressed faults and triggering instabilities (9, 11). However, a growing body of literature suggests that a primary response of faults to fluid-pressurization could also be slow, as eismic slip which, in turn, could transmit the solid stresses that trigger the observed induced seismicity (12–16). Large, spatially extended regions of fluid-activated as eismic slip have been inferred in response to deep fluid injection (at depths greater than 1 km) (13, 16). Such large regions of as eismic slip, in some cases,



are hypothesized to have triggered moderate-sized earthquakes on faults unlikely to be pressurized via fluid migration (16, 17). Yet, whether realistic subsurface hydro-mechanical conditions permit fluid-activated aseismic slip to transfer potentially earthquake-inducing stresses to regions remote from injection activity has never been tested with data-constrained models of fault slip (18).

5

10

15

Models predict that aseismic slip on fluid-pressurized faults can outpace pore-fluid migration under certain conditions (19). Specifically, theoretical studies of injection-induced earthquake nucleation indicate that the pre-injection stress state may influence the aseismic propagation of a rupture front relative to fluid migration (19). However, in the absence of continuous, in situ, measurements of active fault deformation and hydrological processes, the existing observations of the spatio-temporal evolution of fluid-activated aseismic slip are only indirect and rely primarily on seismicity migration or surface geodetic observations (16, 17). This leaves the details of both pore-fluid migration and aseismic slip propagation, and their inter-relationship, ill-constrained. As a result, these model-predicted scenarios and their underlying physics have had limited opportunities to be satisfactorily tested against direct observations of fault hydro-mechanical behavior.

20

Fluid-injection experiments on shallow crustal faults bridge this data gap by activating and directly measuring fluid-induced aseismic slip and pore-pressure evolution at the fault (15). However, we do not know whether observations from a single borehole can constrain models of spatially extended shear ruptures stimulated by pore-fluid migration. We use the experimental data from Guglielimi et al. (15) within a probabilistic inversion framework to estimate the hydro-mechanical parameters of an activated fault and spatio-temporal evolution of slip. The joint measurements of



10

15

20

both pore pressure and slip impose unambiguous constraints on the relationship between porefluid migration and aseismic slip propagation, revealing that the inferred rupture ultimately outpaces pore-fluid migration.

The fluid-injection experiments of Guglielmi et al. (15) activated carbonate faults at depths around 280 m in the Low Noise Underground Laboratory in southeastern France. They injected water with an increasing rate over a period of 1400 s into the target fault zone from a cross-cutting vertical borehole. They recorded pore pressure, flow rate, shear and normal displacement of the fault at the borehole during injection. In response to fluid-injection, the fault accommodated around 1.2 mm of total slip at the borehole. The first ~ 0.3 mm of slip was seismically quiescent, but further slip accumulation was accompanied by seismicity recorded at down-hole seismic sensors in nearby monitoring wells. Gugliemi et al. inferred the slip episode was primarily aseismic because (i) the total accumulated seismic moment was inferred to be a small fraction of the moment estimated from the observed slip and approximated rupture area, and (ii) both the slip and pressure time histories appeared insensitive to the onset of seismicity (15).

Our physical model for this experiment has two coupled components, (i) a hydrological model for fluid flow into the rock formation (Fig. 1A) and (ii) a model for quasi-static rupture of a planar fault (Fig. 1C). We presumed fluid flow was fault-parallel and radially outward from the borehole, on the basis that the slip surface was embedded within a narrow fault damage zone, which provided a compliant conduit with high fluid permeability relative to the surrounding host rock (Fig. 1A) (20). The hydrological model has two parameters: permeability k [m^2] and hydraulic storage S_s [m^{-1}]. The model response to borehole injection is the spatiotemporal evolution of pore fluid



10

15

20

pressure p within the damage zone, which we solved numerically subject to the variable injection rate of the field experiment. We used an adaptive Markov Chain Monte Carlo (MCMC) routine to obtain the full posterior probability distributions for permeability and specific storage (20) given the pore-pressure data of (12) (Fig. 1B). The hydrological model provides a spatio-temporal evolution of pore fluid pressure away from the borehole and along the fault plane. Our model for fault slip is that of a shear rupture driven by the evolving fluid pressure and concomitant local decrease in frictional strength (Fig. 1C). We account for the decrease by assuming that shear strength is the product of the local effective normal stress, the difference between the fault normal stress σ and the local pore fluid pressure p, and a coefficient of friction (17). Our rupture model parameters included the magnitude of the initial fault shear traction τ , initial effective normal traction σ , the host rock shear modulus G_o . We parametrized the friction coefficient by hypothesizing it to either have a constant value f or to linearly weaken with slip from a peak value of f_p to a residual value f_r over a slip scale D_c . The slip at the borehole we predicted with this model was compared to the observed slip (Fig. 1D) to obtain Bayesian constraints on the model parameters using the same MCMC routine applied to the hydrological data.

We compared our hydrological model to the data and inferred that increased permeability was likely to have accompanied fault slip. and we constrain the magnitude of the increase. We found that in response to the volume injection rate history (Fig. 2A), the pore pressure at the well (Fig. 2A) shows multiple instances where non-decreasing injection rate accompanied rapid pressure drops (most prominently at 618 s and 940 s, Fig. S2 in (20)). Our hydrological model, with constant permeability and specific storage, cannot accommodate these observations. As a first-order modification to accommodate this behavior, we allowed the model permeability to undergo step



10

15

20

changes at the times corresponding to these anomalous pressure-drops. The pressure history of our enhanced model captured the observed pressure history with plausible parameter values (Fig. 2A). The permeabilities derived from this 4-parameter model (Fig. 2) required a 60% permeability enhancement across these pressure drops. The permeability magnitudes we determined are consistent with estimates from previous pulse injection tests carried out in the test area ($\sim 10^{-12}$ m²) (21). The magnitude range we determined for specific storage ($10^{-3} - 10^{-5}$ m⁻¹) also overlaps with the range of in situ estimates from fault damage zones ($10^{-4} - 10^{-5}$ m⁻¹) (22, 23). We chose the minimum root-mean-square misfit model from the posterior probability distributions of the parameters (Fig. 2B) as the appropriate description of the spatio-temporal pore-pressure evolution that stimulates the shear rupture. This particular model of ours has a hydraulic diffusivity of 0.04 m²s⁻¹.

The fault permeabilities have a monotonic increase $(k_3 > k_2 > k_1)$ with continued injection without any *a priori* constraints on the parameter inter-relation. Fault-zone permeability varies with shear slip on reactivated faults both in the laboratory (24-26) and in the field (15, 27). Our estimates of the step changes in permeability indicate, however, that permeability enhancement saturates even as slip continues to accumulate at an accelerated rate. The posteriors for k_3 and k_2 overlap to a greater extent than those for k_1 and k_2 in Fig. 2B. This saturation in permeability enhancement, instead, seems to more closely follow the observed leveling of the fault normal displacement after approximately 1000 s of injection reported in (15) (Fig. 1D).

Examining the history of slip at the borehole provides evidence for a slip-weakening description of fault strength, with constraints on the change in friction coefficient and characteristic slip



distance, as well as the host rock shear modulus and in situ stress state. We solve for the evolution of slip at the borehole using our best fit hydrological model. We found that the slip acceleration cannot be captured with the slip predicted by a constant-friction-coefficient model (Fig. S4 in (20)). A potential source of slip acceleration is the weakening of the fault accompanying sliding. Laboratory tests of rocks under triaxial compression suggest that the post-failure strength of initially intact carbonate and granitic rocks reduces approximately linearly with slip (28-30). We choose such piecewise-linear slip-weakening as a simple description of reduction in fault strength. With a slip-weakening friction coefficient, our modeled quasi-static slip at the borehole captured the prominent features of the slip history. Our best-fit model (pink curve in Fig. 3A) reproduced the initial slow accumulation of slip transitioning into the subsequent rapid acceleration beyond 1180 s of injection. However, this fit does not explain the initial, slower acceleration prior to 1180 s. An excellent fit to the first 1180 s of slip alone (yellow curve in Fig. 3A) requires D_c approximately three times as small (0.10 mm as opposed to 0.37 mm, Fig. 3F) and G_o around twice as large (20.71 GPa as opposed to 11.84 GPa, Fig. 3C).

Our data-inferred model has a rupture front that accelerates ahead of a region of substantial pore fluid pressure increase. The three insets in Fig. 3A show the spatial extent of the slip-weakening rupture at three instants of time. The top right inset shows that the slip-parallel extent of the aseismic rupture near the end of fluid-injection is approximately 3 times the size of the region which has been pressurized by 1 MPa or more. The advancement of aseismic slip ahead of fluid migration is due to the large inferred background stress relative to peak strength $(\tau/f_p\sigma\sim 0.64)$ and the large overpressures sustained over the last 600 s of injection. The inferred rupture properties $(\tau > f_r\sigma)$ suggest that it might have ultimately turned dynamic if fluid pressurization was



continued and no other mechanisms initiated (18, 19, 31). Such run-away ruptures might greatly exceed any estimate of the maximum induced earthquake magnitude derived assuming that the stimulated rupture is spatially limited instead by the extent of the fluid-pressurized volume (31, 32). On the other hand, if nucleation is otherwise prohibited, such large assismic ruptures could continue to transmit stresses to regions outside the fluid-pressurized regions. We note that the conditions that allow such rapid growth of assismic slip are not dependent on the absolute stress levels and, therefore, could reasonably be expected to apply to depths greater than that of the Guglielmi et al. (15) experiment.

Aseismic slip on fluid-activated faults can outpace pore pressure diffusion under fairly general frictional strength prescriptions, provided that the fault is nearly critically stressed where the fault-resolved shear stress approaches the pre-injection fault strength. We demonstrate the underlying mechanical principle with a simple, constant-friction model, wherein the fluid-driven rupture front also enlarges diffusively. We considered the in- or anti-plane slip of a fault with a uniform pre-injection state of stress (Fig. 4A), with strength determined by a friction-coefficient f(20). In this scenario, a source of fluid that diffuses along the fault with a hydraulic diffusivity α can drive an aseismic rupture front that also propagates in a diffusive manner. Here, the rupture length grows proportionally to the diffusive length scale for pore-fluid migration, $\sqrt{\alpha t}$. The constant of proportionality, λ , depends on the pre-injection state of stress and strength of the fault (Fig. 4B). Under conditions approaching a critical state of stress, the rupture front will quickly advance well beyond a region of substantial pore pressure increase with $\lambda \gg 1$. Observations from studies of fractures cross-cutting boreholes indicate that the subset of fractures that are hydraulically conductive are also likely to be critically stressed (33–35). This observation combined with our



10

15

20

25

model above suggests that large overpressures created through subsurface fluid injection may activate aseismic slip over regions considerably larger than the pressurized region and transmit solid stresses to regions remote from the injection point. Accordingly, the observed diffusion of induced micro-seismicity away from injection sites may reflect stress perturbations due to aseismic slip of a fluid-conducive fault fracture network, rather than the diffusion of elevated pore fluid pressures (9, 11).

Our study also provides valuable in situ constraints on the physics underlying rupture models in general. Such models of spatially extended fault slip almost exclusively use either remote seismological or laboratory-derived estimates for fault constitutive parameters, in particular for the determination of fault strength. These parameters critically influence fault stability and its hazard potential. Some of these parameters, like the slip weakening distance D_c , show orders of magnitude variation between field-scale seismological ($D_c \approx 0.5$ –1 m, 36, 37) and cm-scale laboratory measurements ($D_c \approx 10^{-6}$ – 10^{-3} m, 38, 39). Our estimates of D_c , and other fault constitutive parameters, show instead that parameter values derived from in situ measurements at the field-scale broadly agree with those derived in the laboratory (40). This provides the first proof-of-concept that such well instrumented 'natural fault laboratories' could help constrain the broader issue of scale-dependence of fault constitutive behavior and, as a result, increase our confidence in the realism of physics-based models of earthquake hazard.

References and Notes

- 1. W. L. Ellsworth, Injection-Induced Earthquakes. *Science*. **341** (2014), doi:10.1785/gssrl.83.2.250.
- 2. M. Weingarten, S. Ge, J. W. Godt, B. A. Bekins, J. L. Rubinstein, High-rate injection is associated with the increase in U.S. mid-continent seismicity. *Science*. **348**, 1336–1340



25

35

(2015).

- 3. K. M. Keranen, M. Weingarten, G. A. Abers, B. A. Bekins, S. Ge, Sharp increase in central Oklahoma seismicity since 2008 induced by massive wastewater injection. *Science.* **345**, 448–451 (2014).
- J. Charléty *et al.*, Large earthquakes during hydraulic stimulations at the geothermal site of Soultz-sous-Forêts. *Int. J. Rock Mech. Min. Sci.* **44**, 1091–1105 (2007).
 - 5. N. Deichmann, D. Giardini, Earthquakes Induced by the Stimulation of an Enhanced Geothermal System below Basel (Switzerland). *Seismol. Res. Lett.* **80**, 784–798 (2009).
 - 6. F. Grigoli *et al.*, The November 2017 M_w 5.5 Pohang earthquake: A possible case of induced seismicity in South Korea. *Science*. **360**, 1003–1006 (2018).
 - 7. K-H. Kim *et al.*, Assessing whether the 2017 M_w 5.4 Pohang earthquake in South Korea was an induced event. *Science*, **360**, 1007–1009 (2018).
 - 8. T. H. W. Goebel, E. E. Brodsky, The spatial footprint of injection wells in a global compilation of induced earthquake sequences. *Science*, **361**, 899–904 (2018).
- 9. S. A. Shapiro, E. Huenges, G. Borm, Estimating the crust permeability from fluid-injection-induced seismic emission at the KTB site. *Geophys. J. Int.* **131**, F15–F18 (1997).
 - 10. M. Schoenball, W. L. Ellsworth, A Systematic Assessment of the Spatiotemporal Evolution of Fault Activation Through Induced Seismicity in Oklahoma and Southern Kansas. *J. Geophys. Res. Solid Earth.* **122**, 10189–10206 (2017).
- 20 11. S. A. Shapiro, E. Rothert, V. Rath, J. Rindschwentner, Characterization of fluid transport properties of reservoirs using induced microseismicity. *Geophysics*. **67**, 212–220 (2002).
 - 12. O. Scotti, F. H. Cornet, In situ evidence for fluid-induced aseismic slip events along fault zones. *Int. J. Rock Mech. Min. Sci.* **31**, 347–358 (1994).
 - 13. F. H. Cornet, J. Helm, H. Poitrenaud, A. Etchecopar, Seismic and aseismic slips induced by large-scale fluid injections. *Pure Appl. Geophys.* **150**, 563–583 (1997).
 - 14. F. H. Cornet, Seismic and aseismic motions generated by fluid injections. *Geomech. Energy Environ.* **5**, 42–54 (2016).
 - 15. Y. Guglielmi, F. Cappa, J. P. Avouac, P. Henry, D. Elsworth, Seismicity triggered by fluid injection-induced aseismic slip. *Science*. **348**, 1224–1226 (2015).
- 30 16. S. Wei *et al.*, The 2012 Brawley swarm triggered by injection-induced aseismic slip. *Earth Planet. Sci. Lett.* **422**, 115–125 (2015).
 - 17. X. Chen *et al.*, The Pawnee earthquake as a result of the interplay among injection, faults and foreshocks. *Sci. Rep.* **7** (2017).
 - 18. T. H. W. Goebel, M. Weingarten, X. Chen, J. Haffener, E. E. Brodsky, The 2016 Mw5.1 Fairview, Oklahoma earthquakes: Evidence for long-range poroelastic triggering at >40 km from fluid disposal wells. *Earth Planet. Sci. Lett.* **472**, 50–61 (2017).
 - 19. D. I. Garagash, L. N. Germanovich, Nucleation and arrest of dynamic slip on a pressurized fault. *J. Geophys. Res. B Solid Earth.* **117**, B10310 (2012).
 - 20. Materials and methods in Supplementary Materials.



15

20

- 21. P. Jeanne, Y. Guglielmi, F. Cappa, Dissimilar properties within a carbonate-reservoir's small fault zone, and their impact on the pressurization and leakage associated with CO2 injection. *J. Struct. Geol.* **47**, 25–35 (2013).
- 22. M. L. Doan, E. E. Brodsky, Y. Kano, K. F. Ma, In situ measurement of the hydraulic diffusivity of the active Chelunepu Fault, Taiwan. *Geophys. Res. Lett.* **33** (2006).
- 23. L. Xue *et al.*, Continuous permeability measurements record healing inside the Wenchuan earthquake fault zone. *Science*. **340**, 1555–1559 (2013).
- 24. M. Gutierrez, L. E. Øino, R. Nygård, Stress-dependent permeability of a de-mineralised fracture in shale. *Mar. Pet. Geol.* **17**, 895–907 (2000).
- W. Wu, J. S. Reece, Y. Gensterblum, M. D. Zoback, Permeability evolution of slowly slipping faults in shale reservoirs. *Geophys. Res. Lett.* **44**, 11368–11375 (2017).
 - 26. K. Im, D. Elsworth, Y. Fang, The influence of preslip sealing on the permeability evolution of fractures and faults. *Geophys. Res. Lett.* **45**, 166–175 (2018).
 - 27. Y. Guglielmi *et al.*, In situ observations on the coupling between hydraulic diffusivity and displacements during fault reactivation in shales. *J. Geophys. Res. Solid Earth.* **120**, 7729–7748 (2015).
 - 28. W. R. Wawersik, C. Fairhurst, A study of brittle rock fracture in laboratory compression experiments. *Int. J. Rock Mech. Min. Sci.* **7**, 561–564 (1970).
 - 29. W. R. Wawersik, W. F. Brace, Post-failure behavior of a granite and diabase. *Rock Mech.* **3**, 61–85 (1971).
 - 30. T. Wong, Shear fracture energy of Westerly granite from post-failure behavior. *J. Geophys. Res. Solid Earth.* **87**, 990–1000 (1982).
 - 31. M. Galis, J. P. Ampuero, P. M. Mai, F. Cappa, Induced seismicity provides insight into why earthquake ruptures stop. *Sci. Adv.* **3** (2017).
- 25 A. McGarr, Maximum magnitude earthquakes induced by fluid injection. *J. Geophys. Res. Solid Earth.* **119**, 1008–1019 (2014).
 - 33. C. A. Barton, M. D. Zoback, D. Moos, Fluid flow along potentially active faults in crystalline rock. *Geology.* **23**, 683 (1995).
 - 34. J. Townend, M. D. Zoback, How faulting keeps the crust strong. *Geology*. **28**, 399–402 (2000).
 - 35. T. Ito, M. D. Zoback, Fracture permeability and in situ stress to 7 km depth in the KTB scientific drillhole. *Geophys. Res. Lett.* **27**, 1045–1048 (2000).
 - 36. S. Ide, M. Takeo, Determination of constitutive relations of fault slip based on seismic wave analysis. *J. Geophys. Res. Solid Earth.* **102**, 27379–27391 (1997).
- 35 K. B. Olsen, R. Madariaga, R. J. Archuleta, Three-Dimensional Dynamic Simulation of the 1992 Landers Earthquake. *Science.* **278**, 834–838 (1997).
 - 38. M. Ohnaka, M. Akatsu, H. Mochizuki, A. Odedra, F. Tagashira, Y. Yamamoto, A constitutive law for the shear failure of rock under lithospheric conditions. *Tectonophysics.* **277**, 1-27, (1997).



10

15

- 39. M. Ohnaka, L.-F. Shen. Scaling of the rupture process from nucleation to dynamic propagation: implications of geometric irregularity of the rupturing surfaces. *J. Geophys. Res.* **104**, 817–844 (1999).
- 40. F. Cappa, M. M. Scuderi, C. Collettini, Y. Guglielmi, J-P. Avouac, Stabilization of fault slip by fluid injection in the laboratory and in situ, *Sci. Adv.* **5** (2019).
- E. Detournay, A. H.-D. Cheng, in Analysis and Design Methods, C. Fairhurst, Ed. (Pergamon, Oxford, 1993; https://www.sciencedirect.com/science/article/pii/B9780080406152500113), pp. 113–171.
- 42. N. J. Salamon, J. Dundurs, Elastic fields of a dislocation loop in a two-phase material. *J. Elasticity.* **1**, 153–164 (1971).
- 43. N. J. Salamon, J. Dundurs, A circular glide dislocation loop in a two-phase material. *J. Phys. C: Solid State Phys.* **10**, 497–507 (1977).
- 44. H. Gao, Nearly circular shear mode cracks. Int. J. Solids Struct. 24, 177–193 (1988).
- 45. F. Erdogan, G. D. Gupta, On the numerical solution of singular integral equations. *Quarterly of Applied Mathematics.* **29**, 525–534 (1972).
- 46. F. Erdogan, G. D. Gupta, T. S. Cook, *Methods of analysis and solutions of crack problems* (Springer Netherlands, 1973), pp. 368–425.
- 47. R. C. Viesca, J. R. Rice, Nucleation of slip-weakening rupture instability in landslides by localized increase of pore pressure. *J. Geophys. Res.: Solid Earth* **117**, B03104 (2012).
- 48. R. C. Viesca, D. I. Garagash, Numerical methods for coupled fracture problems. *J. Mech. Phys. Sol.* **113**, 13–34 (2018).
 - 49. P. Bhattacharya, A. M. Rubin, E. Bayart, H. M. Savage, C. Marone, Critical evaluation of state evolution laws in rate and state friction: Fitting large velocity steps in simulated fault gouge with time-, slip-, and stress-dependent constitutive laws. *J. Geophys. Res.: Solid Earth.* **120**, 6365–6385 (2015).
 - 50. N. Metropolis, A. Rosenbluth, M. N. Rosenbluth, A. H. Teller, E. Teller, Equation of State Calculations by Fast Computing Machines. *J. Chem. Phys.* **21**, 1087–1092 (1953).
 - 51. W. K. Hastings, Monte Carlo sampling methods using Markov chains and their applications. *Biometrika*. **57**, 97–109 (1970).
- 30 52. A. Malinverno, Parsimonious Bayesian Markov chain Monte Carlo inversion in a nonlinear geophysical problem. *Geophys. J. Int.* **151**, 675–688 (2002).
 - 53. W. H. Press, S. A. Teukolsky, W. T. Vetterling, B. P. Flannery, Numerical recipes in Fortran 90 (2nd ed.): The Art of Parallel Scientific Computing (Cambridge University Press, New York, NY, USA, 1996).
- 35 Y. Bai, Convergence of adaptive Markov Chain Monte Carlo algorithms, University of Toronto (2009).
 - 55. Y. Guan, R. Fleissner, P. Joyce, S. M. Krone, Markov Chain Monte Carlo in small worlds. *Stat. Comp.* **16**, 193–202 (2006).
 - 56. G. I. Barenblatt, "The mathematical theory of equilibrium cracks in brittle fracture" in



- Advances in Applied Mechanics, H. L. Dryden, Th. von Karman, G. Kuerti, F.H. van den Dungen, L. Howarth, Eds. (Elsevier, 1962), pp. 55–129.
- 57. B. Lawn, *Fracture of Brittle Solids* (Cambridge Univ. Press, New York, 1993), second edn.
- 5 **Acknowledgments:** The authors thank Frederic Cappa for providing the high-resolution porepressure time history from the field experiments and details of the experimental setup. Funding: This work was supported by the U.S. Geological Survey grant G17AP00016; the National Science Foundation (NSF) grant EAR-1653382; and the Southern California Earthquake Center (SCEC). SCEC is funded by NSF Cooperative Agreement EAR-1033462 and USGS Cooperative Agreement G12AC20038. The experimental data were obtained with funding by the Agence 10 Nationale de la Recherche (ANR) through the HPPP-CO2 project under contract ANR-07-PCO2-0001 and the HYDROSEIS project under contract ANR-13-JS-06-0004-01. Author contributions: R.C.V. contributed to conceptualization, methodology, and writing. P.B. contributed to methodology, formal analysis of data, and writing. Competing interests: Authors declare no competing interests. Data and materials availability: All data used in this work has 15 been made available in the Supplementary Materials of Guglielmi et al. (15). The Fortran library developed for Bayesian inversion is freely available at: pathikrit-bhattacharya, & pathikritb. (2019, April 6). pathikrit-bhattacharya/MCMC fortran library: FortMcMc v1 (Version v1.0.0). Zenodo. http://doi.org/10.5281/zenodo.2631455.

Supplementary Materials:

Materials and Methods Supplementary Text Figures S1-S4

25 References (41-57)

30

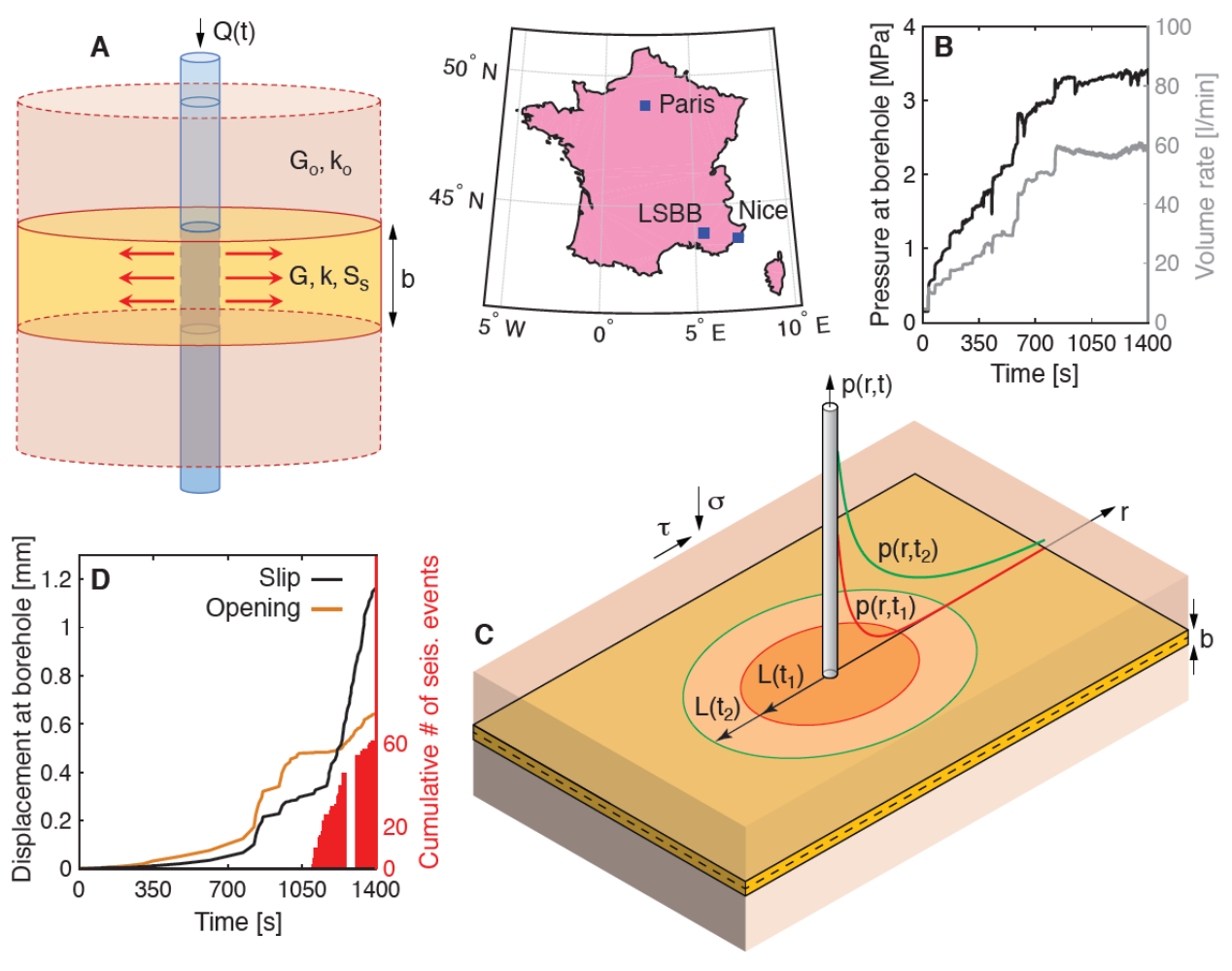


Figure 1: Model schematics and in situ observations of pore-pressure and slip (15): (A) Fluid is injected at an instantaneous volume rate Q(t) through the open section of a borehole into a permeable fault damage zone of width b, permeability k, elastic modulus G and hydraulic storage S_s . The host rock is characterized by permeability k_o and shear modulus G_o . (B) The volume rate injection history (grey) and the observed pressure response at the borehole (black). (C) Shear slip on the planar fault is driven by the background shear stress τ and facilitated by the decrease in effective normal stress $\bar{\sigma} = \sigma - p(r, t)$ as pore pressure p(r, t) builds up; σ is the fault resolved normal stress. The rupture has an instantaneous slip parallel length L(t). (D) The observed fault slip (black) and fault opening (orange) at the borehole, the cumulative count of accompanying micro-seismicity is shown as red bars.



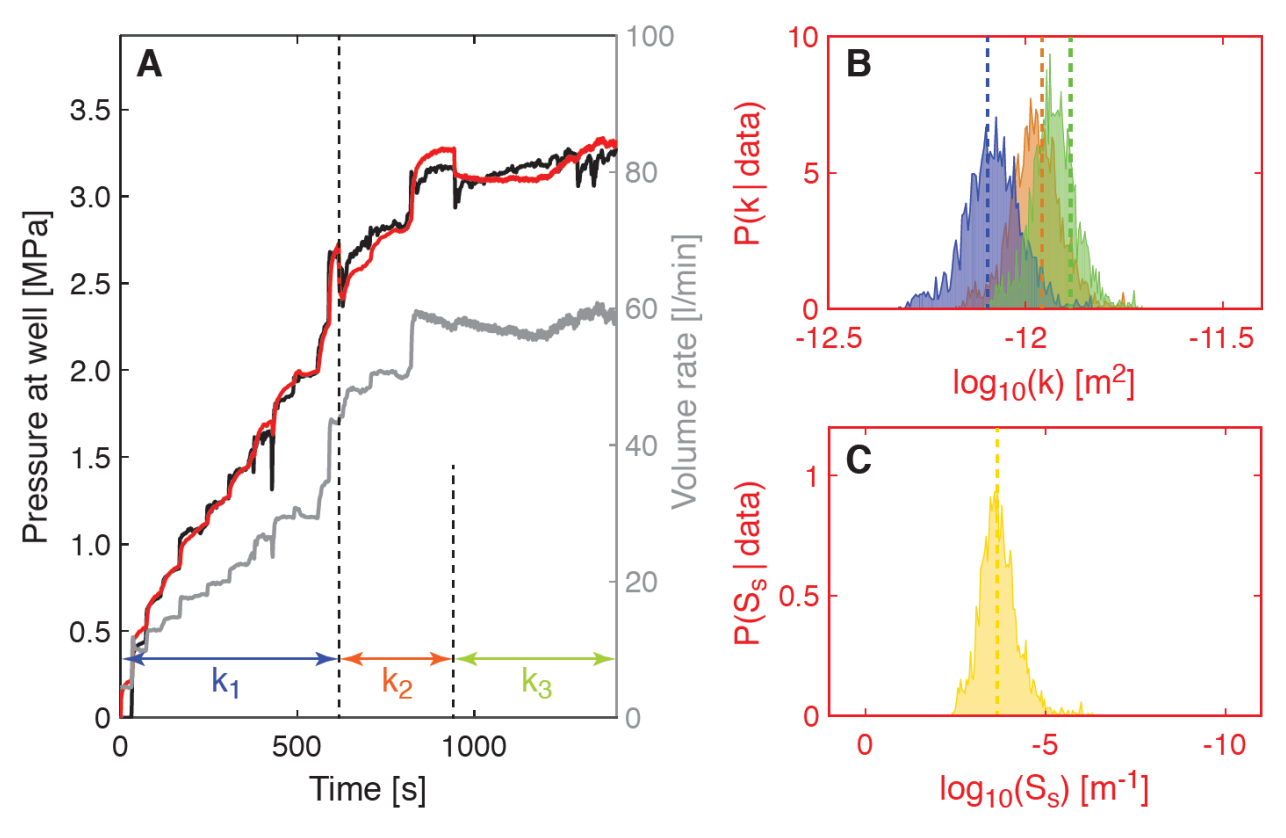


Figure 2: Model comparisons with observed pore-pressure history (black curve in A) at the well in response to the imposed injection history (grey curve in A). (A) The best fit to the pore-pressure time history, with two step changes in permeability (the 4-parameter hydrologic model) at 618 s and 940 s, is shown in red. (B) Posteriors for permeability are shown in blue for k_1 , orange for k_2 and green for k_3 . (C) Posterior for the storage coefficient. The vertical dashed lines in B, C show the parameter values for the best fit model shown in A. The values are $k_1 = 0.8 \times 10^{-12}$ m², $k_2 = 1.1 \times 10^{-12}$ m², $k_3 = 1.3 \times 10^{-12}$ m², and $S_s = 2.15 \times 10^{-4}$ m⁻¹.



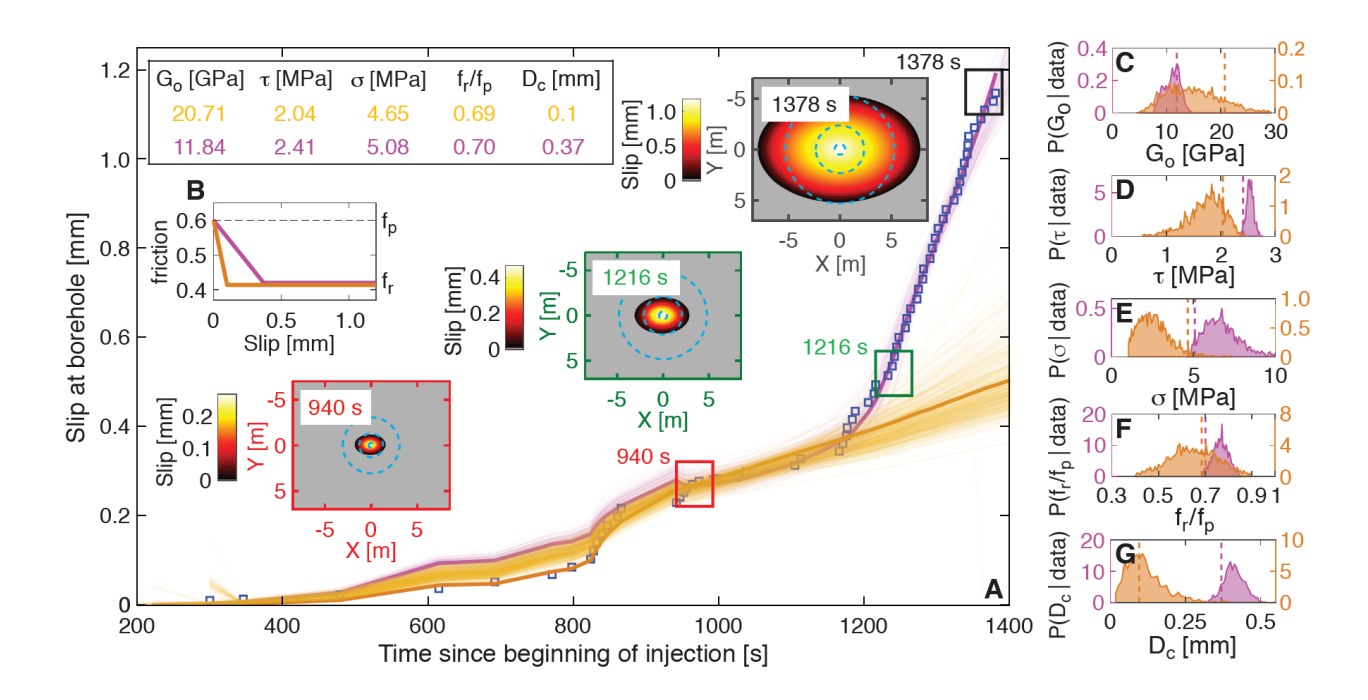


Figure 3: **Fits to the observed slip (blue squares) at the borehole in response to fluid injection** (15). (A) The model time history (purple and orange curves) reflects the slip at the center of nearly elliptical ruptures whose strength is determined by the local effective normal stress and a piecewise-linear slip-weakening friction coefficient with peak strength f_p , residual-to-peak strength ratio f_r/f_p and slip-weakening distance D_c . The shaded regions around the colored lines represent 10% of the accepted samples with shading density representing frequency of occurrence. The purple curve fits the entire time history of slip, the orange curve the first 1180 seconds only. The three contour insets show the spatial distributions of slip corresponding to the purple curve at the indicated times. The dashed blue contours represent increases in pore-pressure by 2, 1 and 0.5 MPa. (B) The linear slip-weakening model derived from the fits in A. (C)–(G) The Bayesian posteriors corresponding to the fits in A. The reported values of G_o and τ are derived assuming $f_p = 0.6$. The vertical dashed lines represent the least misfit models shown in A.



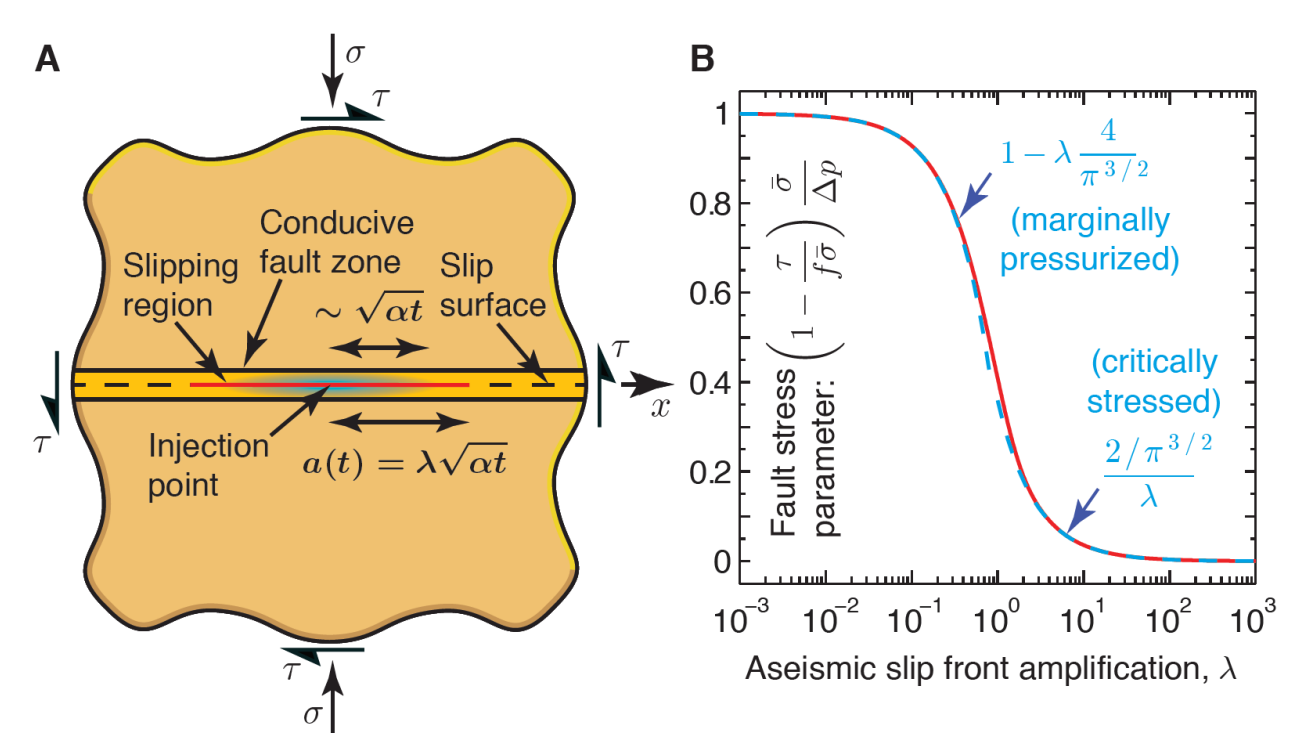


Figure 4: Elementary model of aseismic slip front outpacing fluid migration. (A) Model schematic of an enlarging sliding region of a fault (red) in response to a fluid source within a permeable fault zone. (B) The red curve shows aseismic slip front amplification as a function of the fault stress parameter assuming a constant friction coefficient f and a fluid source of constant amplitude Δp . The blue dashed lines show asymptotic behavior under end-member fault stress regimes. The front of the sliding region leads fluid diffusion ($\lambda > 1$) if the fault is critically stressed (20).